2011 IEEE Radar Conference, Kansas City, Missouri, USA, May 23–27, 2011

Nonseparable Nth-Band Filters as Overlapping-Subarray Tapers

Jeffrey O. Coleman
Naval Research Laboratory
Radar Division
Washington, DC

***Abstract*— In a receive array "overlapped subarrays" refers to an array output formed as a weighted sum of subarray outputs themselves formed as identically weighted combinations of the outputs of overlapping element subsets. The system array factor becomes a product of two array factors with different periods, one associated with each sum, just as the frequency response of a two-stage IFIR filter in a DSP system is the product of two frequency responses with different periods. It is well known that an Nth-band filter can be the most efficient choice for an IFIR filter's first stage, but the corresponding array idea appears unknown.**

Design examples apply modern optimization to nonseparable tapers, with three of four examples featuring Nth-band subarray tapers. Whether an Nth-band approach is best is not settled here and is properly context dependent: designs should be carried out both ways and compared. Further, a very small subarray taper can easily be Nth-band entirely by accident, so designers should be aware of the associated array-factor features that necessarily result and cannot be optimized away.

I. Background and Introduction

A. Review of overlapped subarrays

In the overlapped-subarray receive-array architecture of Fig. 1, identically weighted sums of (typically few) signals from overlapping element subsets become subarray outputs. The array output is a final weighted sum of those (typically many) subarray outputs. While design of the detailed Fig. 2 example used an optimal approach discussed below, a simple two-step design approach is more typical.

The first step designs the final array factor of Fig. 2(a), the Fourier transform of the final taper (summing weights) of Fig. 2(e), to fix the mainlobe shape. (More below about its apparently unreasonable width.) The small period of that final array factor replicates the mainlobe to create the two grating lobes of Fig. 2(a). The second step designs the subarray array factor, the Fourier transform of the subarray taper of Fig. 2(d), to suppress those grating lobes in the product of the final and subarray array factors, the system array factor of Fig. 2(b).

Instead of one final sum there are typically several in parallel, creating several array outputs or "beams." Their final array factors likely have narrower main beams than in Fig. 2(a) and are often identical except for horizontal translation. Five narrow mainlobes of five output beams might, for example, appear where the five peaks of the wide example mainlobe are in Fig. 2(a). Here that wide mainlobe stands in informally for such a cluster of five narrow mainlobes, with the subarray array factor suppressing the grating lobes of each. (More precise illustration of a beam cluster is deferred to the 2D examples of Figs. 4 through 7.) Element-output phase shifts not shown in Fig. 1 (but see vector $\mathbf{k}_c$ in the Appendix's detailed formulation) can steer the cluster as a unit by translating all array factors in lockstep.

B. IFIR filters

It is well known that when subarraying is not used the mathematics of a uniform line array are exactly those of a 1D FIR filter. The array factor is just the filter frequency response with sample spacing T and temporal frequency f replaced respectively with element spacing d and spatial frequency k. The array output in response to a plane wave incident at angle θ from the normal to the array line becomes just the response of the single (embedded) element at the origin scaled by that array factor evaluated at $k = \frac{1}{\lambda}\sin\theta$, the projection onto the array line of the negative of the wavenumber vector (in cycles/length).

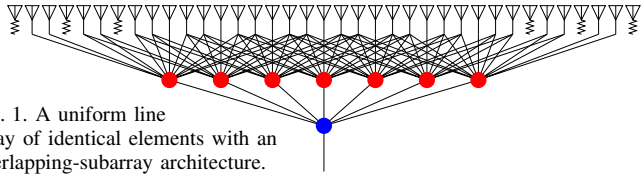

Fig. 1. A uniform line array of identical elements with an overlapping-subarray architecture.

Less appreciated is that the overlapped-subarray architecture relates in the same way to the two-stage version of an interpolated-FIR (IFIR) filter [1], a multi-stage digital-filter structure widely used for its computational efficiency when sharp cutoffs are required. In IFIR-filter terms, the small-period frequency response of the shaping filter in Fig. 2(a) is given the desired passband shape and steep rolloff. The large-period frequency response of an interpolation filter then suppresses periodically repeated passbands to give the frequency response of the two-filter cascade of Fig. 2(b), the IFIR filter, the desired features. The frequency responses of Fig. 2(a) are the Fourier transforms of the impulse responses of Figs. 2(d) and 2(e).

The example filters of Fig. 2 were designed by alternately solving a linear program (LP) for the interpolation filter and a second-order cone program (SOCP) for the shaping filter. LP and SOCP optimization pushed where indicated by $\downarrow$ and $\updownarrow$ in Fig. 2(b) while enforcing bounds flagged by $\longleftarrow$. The approach roughly parallels the [2, Fig. 4] 1D example and exactly parallels the 2D approach of Figs. 9 and 10(a) in this paper's Appendix. Coding used the Opt matlab toolbox [2], [3] interfaced to the SeDuMi numerical solver [4], [5]. Convergence, in under a second, used three LP/SOCP cycles.

C. Nth-band filters

One property of the Fig. 2(a) interpolation filter is not required but is convenient for both IFIR filters and overlapped subarrays: it is a thirdband filter, an *Nth-band (Nyquist) filter* with $N = 3$. A 1D filter is Nth-band if its impulse response h_n has zero-valued "Nyquist samples," h_{Nn} for $n \neq 0$. Equivalently, its frequency response $H(fT)$ yields a constant "Nyquist sum" $\sum_{k=0}^{N-1} H(fT - k/N)$. Typically one term dominates, so its passband spans roughly $1/N$ of a period.

In both IFIR filters and overlapped-subarray systems an Nth-band property pairs a useful impulse-response condition with a harmless frequency-response or array-factor condition. Zero impulse-response samples save computation in an IFIR filter and save summing hardware in an overlapped-subarray system, where that analog hardware must be duplicated for every subarray output. Each such sample

This work was supported by the Naval Research Laboratory base program.
Author contact info at http://alum.mit.edu/www/jeffc

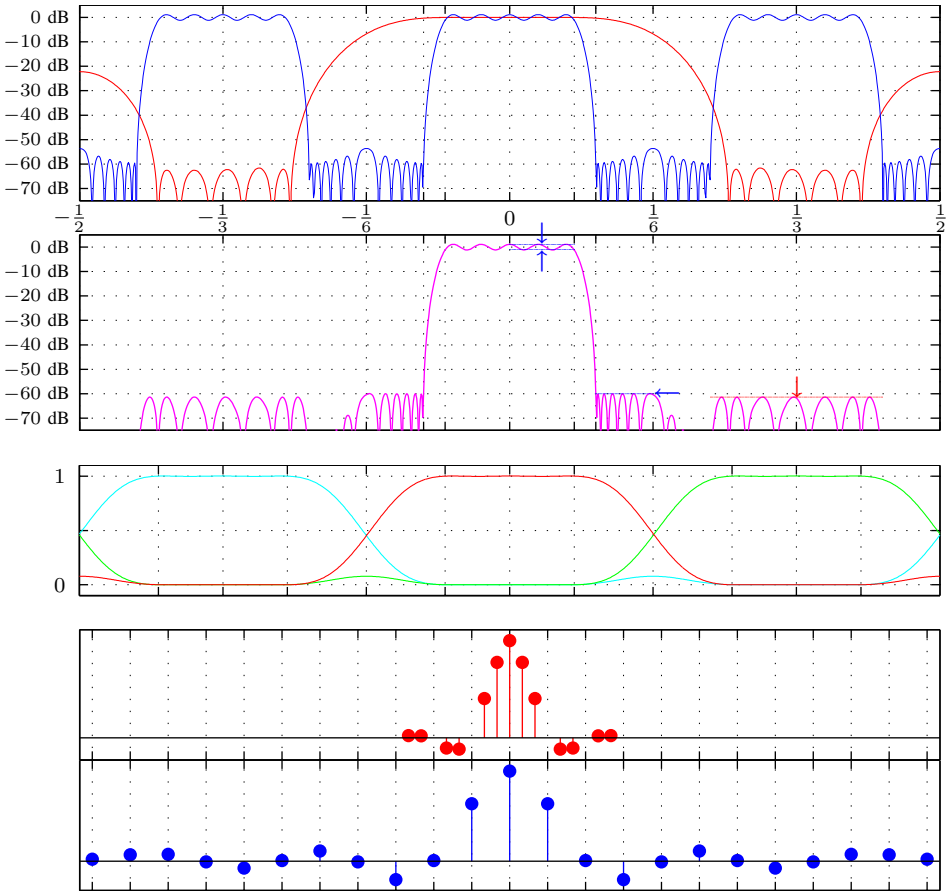

Fig. 2(a). Example magnitudes of a line array's final and subarray array factors or, equivalently, magnitude responses of an IFIR filter's shaping and interpolation filters, plotted versus normalized frequency, for the filters fT and for the array factors kd, the latter with k denoting spatial frequency along a line of d-spaced elements.

Fig. 2(b). Magnitude response of the system array factor of a line array with the final and subarray array factors of Fig. 2(a) or, equivalently, of an IFIR filter comprising the shaping and interpolation filters of Fig. 2(a). Arrows and lines of tiny dots represent the iterative LP/SOCP filter-optimization strategy used to design the two components in Fig. 2(a).

Fig. 2(c). The periodic frequency response, on a linear scale, of the subarray array factor or interpolation filter of Fig. 2(a) and its translations in normalized frequency by $\frac{1}{3}$ and $\frac{2}{3}$. The three curves sum to unity, so the filter is a thirdband filter. (Figure 3 shows the analogous 2D idea.)

Fig. 2(d). The above design's subarray taper or interpolation-filter impulse response. Because it happens to be a thirdband filter—this is not required—it is zero at multiples of three samples except at the origin.

Fig. 2(e). The above design's final taper or shaping-filter impulse response, supported on every third sample only to reflect the element-to-subarray density ratio along the array line or the interpolation factor in the IFIR filter.

zeroed removes a degree of optimization freedom, but the restriction is only enough to force a constant Nyquist sum. When N is also the interpolation factor, that is nearly harmless, because the stopbands required to suppress repeated passbands or grating lobes imply, through the constant Nyquist sum, a passband exactly where needed.

In these applications the major real cost of fixing the Nyquist sum is twofold. First, the freedom to trade off passband and stopband accuracies is lost. The small stopband response required typically maps through the Nyquist sum to a passband response flatter than needed, and the implicit overdesign can necessitate a marginally longer impulse response than would be needed to meet the actual passband requirement absent the Nth-band property. Second, losing flexibility in the transition band can also entail costs. In the transition band the Nyquist sum typically has just one or two nontrivial terms, and summing those terms to the passband height then means that the frequency response or array factor is about 6 dB down when fT or kd is $\pm\frac{1}{2N}$. This is visible in a rough way at $\pm\frac{1}{6}$ in Fig. 2(a). It is visible more precisely at $\frac{1}{6}$ in Fig. 2(c), where the two dominant terms cross just below $\frac{1}{2}$ because the third term is just above zero. Some performance costs can be overcome with a longer impulse response.

Whether the Nth-band approach yields a net win, because of the zero impulse-response samples, or a net loss, due to the extra impulse-response length needed, cannot be known *a priori*. Designs with and without the Nth-band feature must be completed and compared.

D. This paper

This paper presents the Nth-band idea for 2D tapers, to inform and improve subarray-taper design. Examples are favored over mathematics, which is adequately developed elsewhere [6]. The Appendix presents the formulations used to optimize tapers in example designs.

II. The Overlapped-Subarray Architecture in 2D

A. The correspondence between the 2D case and the earlier 1D case

In Fig. 2(e) the samples of the final taper are contained in a uniformly spaced discrete subset of the array line. That subset is contained in another such set, $N=3$ times more dense, that contains the sample locations of both the subarray taper and the convolution of the two tapers. (That convolution determines element positions.)

A 2D taper has sample locations contained in an array-plane lattice, a discrete point set closed under vector addition and negation that generalizes on the uniformly spaced sample positions of Fig. 2. In each of Figs. 4(a), 5(a), 6(a), and 7(a) sample locations are shown for the final taper, the subarray taper, and their convolution, the system taper. Samples of the final taper are confined to a sublattice (subset of a lattice that is itself a lattice) of the element-position lattice that contains the sample locations of the other two. *The subarray taper is an Nth-band filter if it has no samples on that final-taper sublattice except the sample at the origin.* The subarray tapers of Figs. 4(a), 5(a), and 6(a) are Nth-band. The subarray taper of Fig. 7(a) is not.

The array factors are now 2D. In Figs. 4(b), 5(b), 6(b), and 7(b) the lower-left array factors are analogous to the final array factor in Fig. 2(a). Magnitude in dB is now color coded, and a black -3 dB contour line marks the passband / mainlobe / main beam centered at boresight, the center of the visible-region globe of azimuth-elevation coordinates. That main beam and its periodic replicas are centered in array-factor periods demarcated by straight lines.

These lower-left array factors have such small periods that array-factor translation to steer that main beam to the edge of the visible region would make its replicas visible and therefore into grating lobes. The upper-left array factors are analogous to the subarray array factor in Fig. 2(a), and each has both a larger period and stopbands

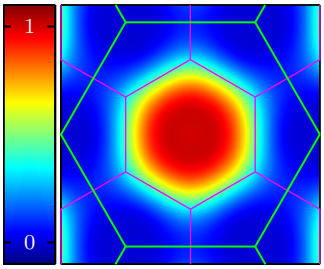

Fig. 3. Frequency response, on a linear amplitude (color) scale, of the 2D thirdband filter used as a subarray array taper in Fig. 5. Here a large hexagonal period comprises one each (net) of three types of small hexagonal subcells that sum to unity when translated into alignment in a 2D equivalent of the Fig. 2(c) idea.

/ sidelobe regions where needed to suppress these potential grating lobes if it and the final array factor are steered in lockstep by realizing that *cluster steering* at the element outputs. Figure 3 shows the effect on an Nth-band array factor of fixing the 2D Nyquist sum at unity.

The product of the two array factors on the left appears at the upper right and is analogous to the system array factor of Fig. 2(b). The latter's wide beam that stands in for multiple narrow beams becomes a single narrow beam in the 2D plots, where dots are analogous to the locations of the tiny Fig. 2(b) dots at the ← symbol, points where inner-sidelobe magnitudes were subject to a fixed upper bound in final array factor optimization. Taper-symmetry constraints implicitly rotate and reflect the dot region across a much larger area, encircling the main beam, where those dot bounds are actually effective.

On the lower right is the maximum dB magnitude of the cluster's system array factors, each created from an unsteered subarray array factor and a final array factor subjected to *intra-cluster steering* at subarray outputs. The dots are analogous to the locations of the tiny Fig. 2(b) dots below the ↓, points where grating-lobe magnitudes were subject to an upper bound in subarray array factor optimization. Array-factor periodicity and symmetry-constraint reflections and rotations made these bounds effective over larger regions that cover every grating lobe completely. The ↓ bound was minimized in Figs. 4, 5, and 6 but was a fixed bound in Fig. 7 (see Section B.4).

B. The individual 2D design examples and the lessons they impart

These hypothetical radar arrays feature large beams, suitable for subsequent adaptive and position-estimation processing, and large clusters for fast volume surveillance. This also sizes features of arrays and array factors conveniently for plotting. The challenge of suppressing large grating lobes favors subarray outputs only modestly less dense than the elements, raising an interesting question: can an overlapped-subarray architecture with such a small density ratio reduce the number of fully processed subarray outputs sufficiently relative to the element count to justify the subarraying hardware?

1) Ultra-simple system's subarray taper is accidentally Nth-band: The Fig. 4 design, on a tilted square element lattice with $\lambda/2$ spacing, uses only a 2:1 lattice density ratio. Five-element subarrays are centered on the 97 sublattice points at or within $\sqrt{29/2}\lambda$ of array center, yielding 217 elements and so an element/subarray ratio ≈ 2.24. The furthest-apart elements have centers separated by $\sqrt{73}\lambda \approx 8.54\lambda$. Intra-cluster steering and the final sum for the cluster's nine beams can be realized jointly as specific outputs of a 16×16 point 2D FFT of subarray outputs [7]. Tapers and array factors are eightfold symmetric—four rotations (including the identity) and four reflections. The halfband subarray taper's fixed center weight of 1/2 leaves just one weight to optimize or even choose by hand. Of course the single degree of freedom and the halfband property each preclude independent design of passband and stopband shapes.

2) A classic Nth-band design and a larger cluster: In Fig. 5 a $\lambda/\sqrt{3}$ spaced hexagonal element lattice and a 3:1 density ratio puts subarray array-factor stopbands in deep holes of the passband periodicity lattice to enable a large, 19-beam cluster some 25° wide, again using selected outputs of a 16×16 point 2D FFT for intra-cluster steering and final summation. A 25-sample thirdband (see Fig. 3) subarray taper yields 52.1 dB grating-lobe suppression. Each taper is invariant with respect to twelve symmetries, six rotations (including the identity) and six reflections. Given the subarray taper's symmetry and its fixed center weight of 1/3, exactly four subarray weights must be chosen (compare Fig. 5(a) with Fig. 8 in the Appendix). Centering subarrays on the 85 sublattice points at or within $\sqrt{21}\lambda$ of array center yields 367 elements for an element/subarray ratio ≈ 4.3 and maximum center-to-center element spacing of $\sqrt{448/3}\lambda \approx 12.22\lambda$. This design is a benchmark for the two that follow.

3) Make an Nth-band taper sparser and tackle a larger cluster: The design above has $[x_1, x_2, x_3] = [0.13647, -0.0037418, -0.011219]$ in the Fig. 8 subarray taper. With $|x_2|$ so much smaller than $|x_1|$, $|x_3|$, or center weight $\frac{1}{3}$, simply setting $x_2 = 0$ and reoptimizing is tempting. The resulting design, in Fig. 6, cannot be fairly compared to that of Fig. 5, however, because the cluster size here is an enormous 37 beams spanning over 30° in azimuth! Even so, grating-lobe suppression of 38.9 dB is obtained. Taper losses are similar, ranging from 2.15 dB to 2.22 dB across the cluster. Beam-center values of the cluster's system array factors range from −0.033 dB to 0.051 dB.

4) A alternative that is not Nth-band: Let us place subarray taper samples on the 19 lattice points nearest array center. This implies six fewer elements and a maximum center-to-center element spacing some 6.9% lower at $\sqrt{388/3}\lambda \approx 11.37\lambda$. The subarray array factor's passband shape is no longer implied by its stopband shape, so, mirroring the strategy used for the final taper, the subarray taper is designed here by minimizing the cluster's worst taper loss subject to the −38.9 dB bound obtained above on the grating-lobe peak.

Convergence to the Fig. 7 result is slower, requiring 30 cycles of optimizing the two tapers. Each of the 37 beams relates via reflection and rotation to one of six representative beams, which have taper losses of 1.09, 1.12, 1.18, 1.22, 1.35, and 1.48 dB, lower than in the above hexagonal-lattice designs but also varying more beam to beam. This variation appears to be due to the subarray array factor's aggressive rolloff, just outside the cluster, into a large null ring. That rolloff lowers beam noise gain and varies beam to beam, and so then do taper losses and system array factors at beam centers, now −0.39, −1.19, −1.60, −2.89, and −3.80 dB. Individual beam scaling mitigates the latter both in Fig. 7(b) and in optimization. However, implementation errors in the weights of the subarray taper are likely to affect the transition bands of the subarray array factor here much more than those errors will affect the flat passbands of Nth-band designs. This may make noise performance across the cluster more sensitive to errors here than in the other designs.

III. Concluding Observations

Design examples here suggest that overlapped-subarray architectures may be viable for receive arrays with huge beam clusters.

In one comparison, Fig. 6 vs. Fig. 7, making the subarray taper Nth-band makes taper losses marginally worse (with other performance parameters fixed) but provides much greater beam-to-beam performance consistency and perhaps—this is reasonable conjecture not demonstrated here—better robustness to weight errors. These observations relate to a single example, however, and cannot be taken as general truths. Designing both ways in the very specific context of the intended system is the only way to know whether the Nth-band characteristic is better present or absent.

It is natural also to occasionally create an Nth-band design by accident, and this must be accounted for in configuring an optimization.

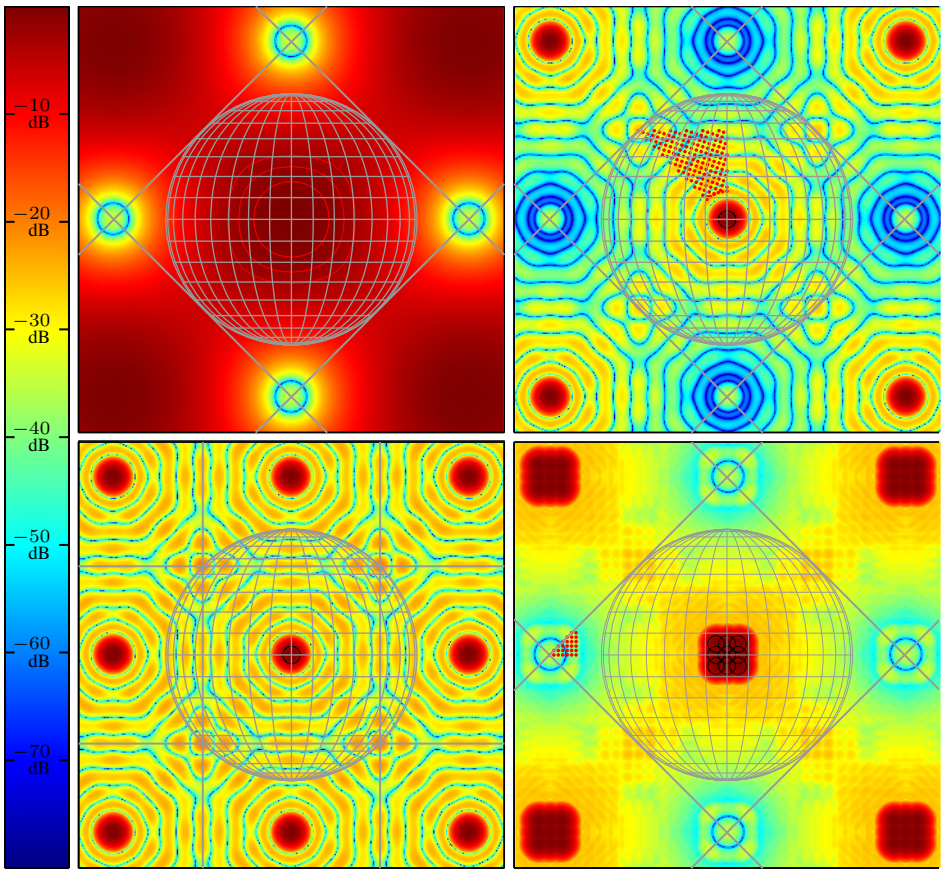

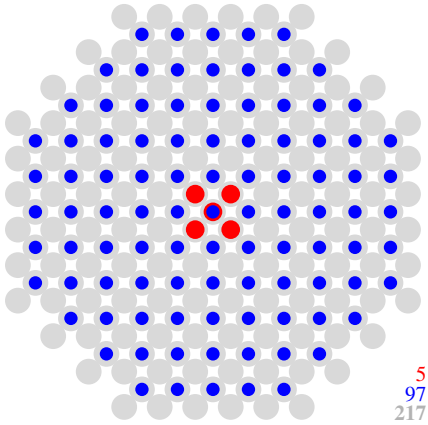

Fig. 4(a). Sample locations of the subarray taper (●), the final taper (●), and their convolution (●). The latter determines element locations.

Fig. 4(b).

subarray	system
final	cluster

3 dB beamwidth 7.86°
max taper loss 0.56 dB

Array-factor magnitudes. The halfband subarray array factor's stopbands allow only half the final array factor's passbands into the system array factor, shown on the right both alone and as a "cluster" computed as the max over nine variants, each with the final taper phase shifted to steer the final array factor. Visible-region globe coordinates are az-el angles. Contours are plotted at -1, -2, and -3 dB over the subarray array factor and at -3 dB over the other array factors. Dots flag where inner sidelobes were bounded to -25 dB and where a minimized grating-lobe bound settled at -34.1 dB.

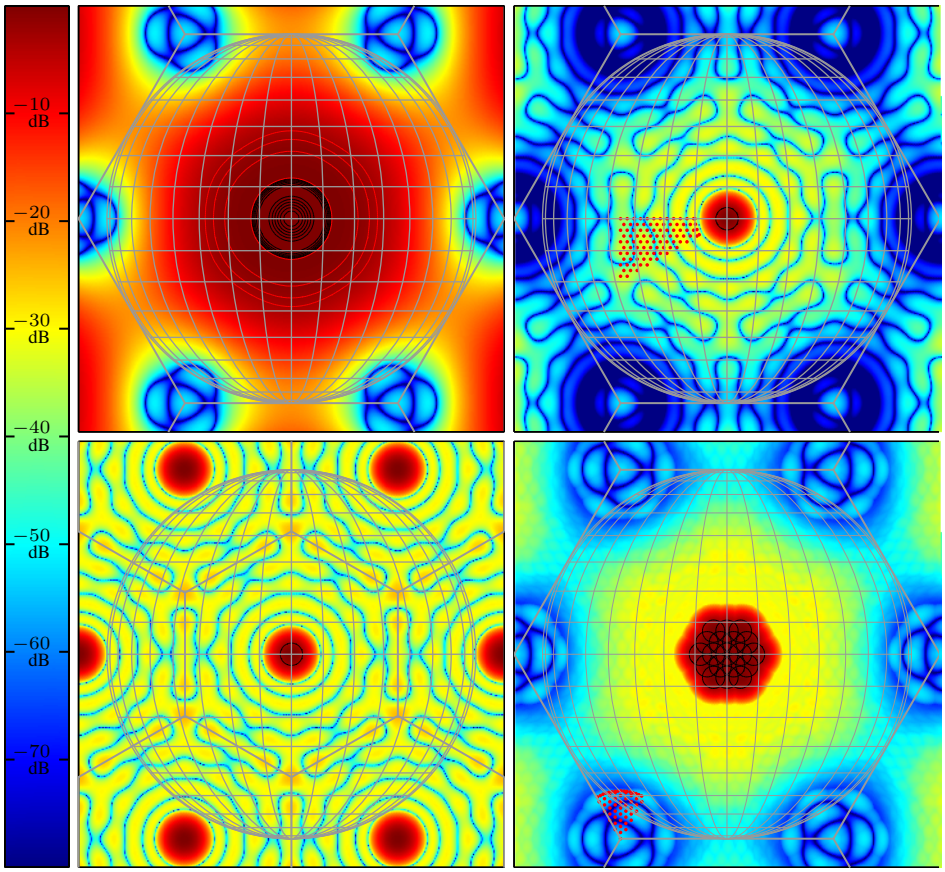

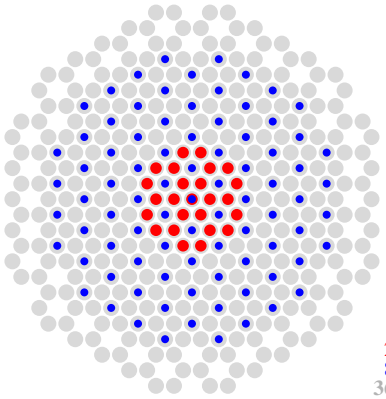

Fig. 5(a). Sample locations of the subarray taper (●), the final taper (●), and their convolution (●). The latter determines element locations.

Fig. 5(b).

subarray	system
final	cluster

3 dB beamwidth 6.95°
max taper loss 2.20 dB

This design features a 19-beam cluster and a thirdband subarray array factor. The latter's two stopbands per period allow only a third of the final array factor's passbands into the system array factor. The taper loss is greater than in Fig. 4 due both to dropping the inner-sidelobe bound here to -30 dB and to a subarray taper here that is much larger relative to the array size. Contours on the subarray array factor are shown at $\{0, -1, -2, -3\}$ dB and at $\{0.01, 0.02, 0.03, 0.04, 0.05, 0.06\}$ dB.

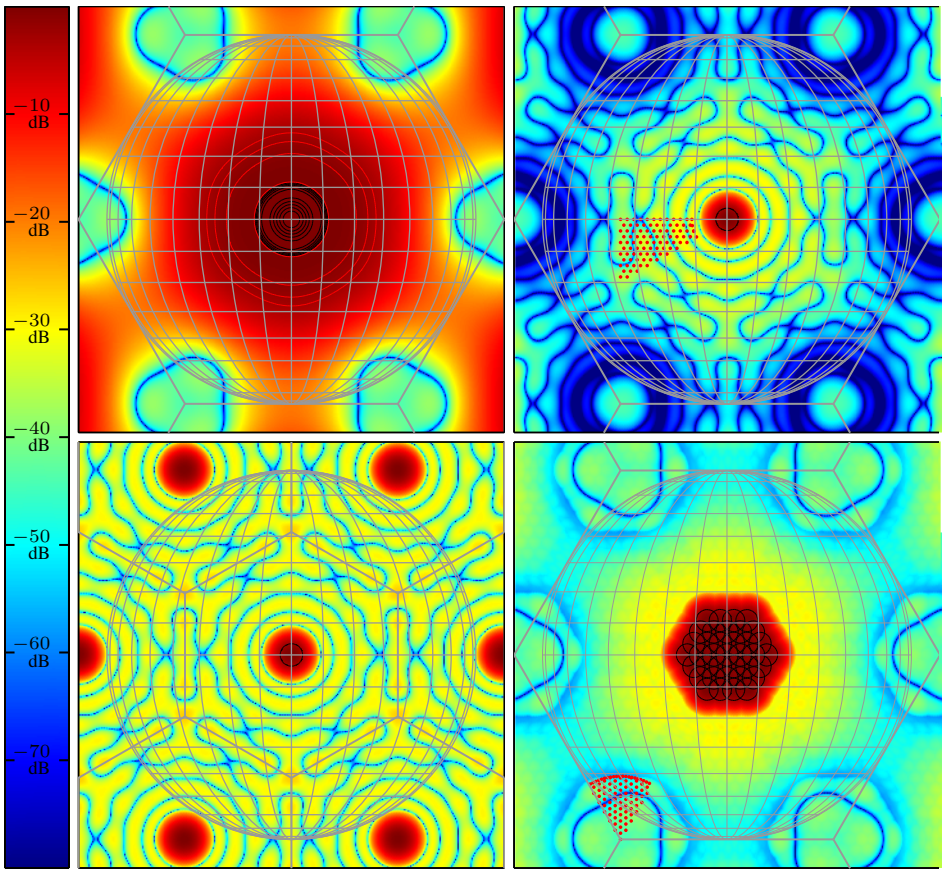

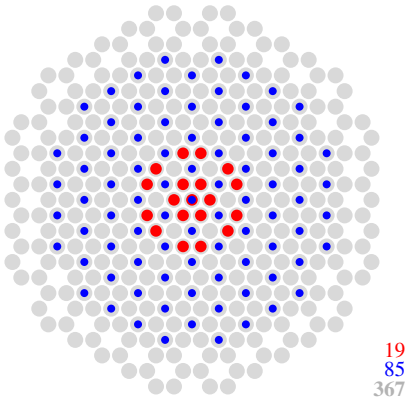

Fig. 6(a). Sample locations of the subarray taper (●), the final taper (●), and their convolution (●). The latter determines element locations.

Fig. 6(b).

subarray	system
final	cluster

3 dB beamwidth 6.97°
max taper loss 2.22 dB

An aggressively sparse thirdband subarray taper suppresses grating lobes of an enormous 37-beam cluster to −38.9 dB while duplicating the beamwidth and taper-loss performance of the Fig. 5 design. Contours on the subarray array factor are at $\{0, -1, -2, -3\}$ dB and at $\{0.01, 0.02, 0.03, 0.04, 0.05\}$ dB.

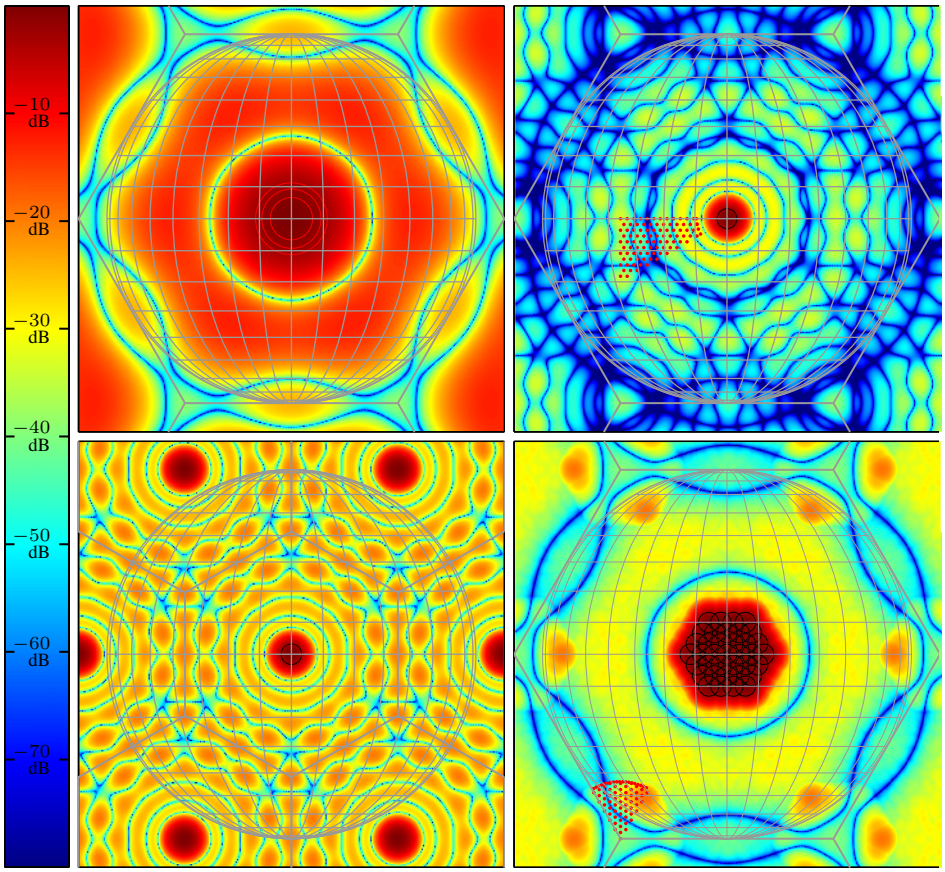

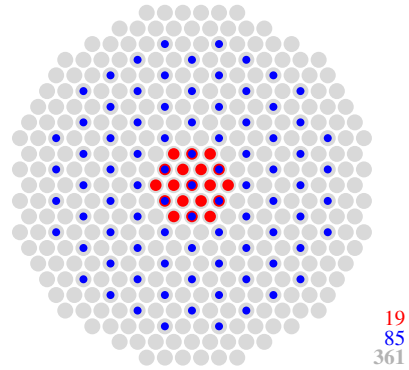

Fig. 7(a). Sample locations of the subarray taper (●), the final taper (●), and their convolution (●). The latter determines element locations.

Fig. 7(b).

subarray	system
final	cluster

3 dB beamwidth 6.09°
max taper loss 1.48 dB

grating lobe peak fixed at −38.9 dB. This array features a 37-beam cluster and a non-Nth-band subarray array factor. Contours on the subarray array factor are at $\{-1, -2, -3\}$ dB. Center-beam beamwidth, reported above, is considerably smaller than in Figs. 5 and Fig. 5 and 6. This is because here more of the sidelobe-suppression burden is borne by the subarray array factor, allowing more of the final array factor's degrees of freedom to be devoted to beam shaping during the optimization process.

APPENDIX
FORMULATION AND OPTIMIZATION

The system array factor [6], [7] is the product

$$\underbrace{H_1\big((\mathbf{k}-\mathbf{k}_c)\mathbf{D}\big)}_{\text{subarray array factor}}\ \underbrace{H_2\big((\mathbf{k}-\mathbf{k}_c-\mathbf{k}_b)\mathbf{DR}\big)}_{\text{final array factor}} \tag{1}$$

(beamspace argument; cluster-center position; beam offset in cluster)

given in terms of the discrete-position Fourier transforms

$$H_1(\boldsymbol{f}) = \sum_{\boldsymbol{n}\in\mathbb{Z}^2} h_1(\boldsymbol{n})\, \mathrm{e}^{-\mathrm{j}2\pi \boldsymbol{f}\boldsymbol{n}}, \quad H_2(\boldsymbol{f}) = \sum_{\boldsymbol{n}\in\mathbb{Z}^2} h_2(\boldsymbol{n})\, \mathrm{e}^{-\mathrm{j}2\pi \boldsymbol{f}\boldsymbol{n}}$$

($\boldsymbol{f}$: dimensionless real row two-vector)

of the subarray taper $h_1(\boldsymbol{n})$ and final taper $h_2(\boldsymbol{n})$, each nonzero only for a finite number of length-two integer column index vectors $\boldsymbol{n}$. Those array factors of course use the same geometry parameters $\mathbf{D}$ and $\mathbf{R}$ as the array-output computation those array factors imply:

$$\text{array output for beam at } \mathbf{k}_c+\mathbf{k}_b = \sum_{\boldsymbol{n},\boldsymbol{m}\in\mathbb{Z}^2} h_2(-\boldsymbol{n})\, \underbrace{\mathrm{e}^{-\mathrm{j}2\pi \mathbf{k}_b\mathbf{D}\mathbf{R}\boldsymbol{n}}}_{\text{intra-cluster steering}} h_1(\mathbf{R}\boldsymbol{n}-\boldsymbol{m})\, \underbrace{\mathrm{e}^{-\mathrm{j}2\pi \mathbf{k}_c\mathbf{D}\boldsymbol{m}}}_{\text{cluster steering}} s(\boldsymbol{m})$$

(length-dimensioned columns are element-position basis vectors; dimensionless 2×2 integer decimation matrix; output of element at position $\mathbf{D}\boldsymbol{m}$)

Array factors (1) scale the embedded element's response to incident plane waves with radian wavenumber vector $-2\pi\mathbf{k}$. In array-factor plots position represents $\mathbf{k}$'s array-plane component, and the visible-region globe of azimuth and elevation coordinates has radius $1/\lambda$.

Figures 8, 9, and 10 present the example designs' optimization strategies. Optimization variables and functions of them are different in color. Finite set $\mathcal{S}$ contains intra-cluster $\mathcal{S}$teering vectors $\mathbf{k}_b$ and so defines the cluster, and finite sets $\mathcal{I}$ and $\mathcal{G}$ contain the points $\mathbf{k}$, dots in the upper- and lower-right plots respectively in each array-factor figure, at which the $\mathcal{I}$nner-sidelobe and $\mathcal{G}$rating-lobe upper bounds of $20\log_{10} b$ and $20\log_{10} g$ (or $20\log_{10} g$) decibels are enforced. Bounds are explicit on "pie slices" of such dots only, but the Fig. 8 symmetry effectively extends the bounds to the "whole pies."

In each of Figs. 9 and 10(b), SOCP taper-loss amplitude factor ℓ bounds a ratio. The numerator is a noise-to-signal amplitude ratio (NSAR), and the denominator is the bound on that NSAR given by the famous inequality of Cauchy, Schwartz, and Bunyakovsky, so that $\ell \geq 1$. In the NSAR expressions N is the number of net-nonzero-weighted array elements, and squared L_2 norm $\|G(\,\cdot\,)\|^2$ is the average of periodic frequency-domain function $|G(\,\cdot\,)|^2$ and is easily computable in the position domain using Parseval's relation.

REFERENCES

[1] Y. Neuvo, D. Cheng-Yu, and S. Mitra, "Interpolated finite impulse response filters," *IEEE Trans. Acoustics, Speech and Signal Processing*, vol. 32, no. 3, pp. 563–570, June 1984.

[2] J. Coleman, D. Scholnik, and J. Brandriss, "A specification language for the optimal design of exotic FIR filters with second-order cone programs," in *IEEE Asilomar Conf. on Signals, Systems, and Computers*, Nov. 2002.

[3] D. P. Scholnik and J. O. Coleman. "Opt matlab toolbox." Naval Research Laboratory. Available online: http://www.scholnik.info/opt.html.

[4] J. F. Sturm, "Using SeDuMi 1.02, a Matlab toolbox for optimization over symmetric cones," *Optimization Methods and Software*, vol. 11–12, pp. 625–653 (versions 1.02/1.03), 1999, updated for version 1.05 online in 2001 (http://www.optimization-online.org/DB_HTML/2001/10/395.html).

[5] I. Pólik and T. Terlaky. SeDuMi 1.21. Cor@l Lab: Computational Optimization Research at Lehigh (http://sedumi.ie.lehigh.edu/).

[6] J. Coleman, K. McPhail, P. Cahill, and D. Scholnik, "Efficient subarray realization through layering," in *Antenna Applications Symp.* (http://www.ecs.umass.edu/ece/allerton/, Monticello IL, USA, Sept. 21–23, 2005.

[7] J. O. Coleman, "Planar arrays on lattices and their FFT steering, a primer," Naval Research Laboratory, NRL Report NRL/FR/5328--11-10,207, est. March 2011.

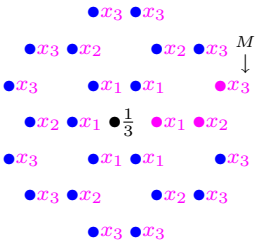

Fig. 8. Each taper (and therefore array factor) is made structurally symmetric by reuse of optimization variables so that only some number M of samples ● can really have their values set independently. Futher, for Nth-band tapers in particular the center sample ● is fixed to the ratio of the lattice densities before and after decimation, as in this example.

Initially let $H_2^{\text{fixed}}(\boldsymbol{f}) = 1$, and

$\forall$ intra-cluster steering direction $\mathbf{k}_b \in \mathcal{S}$,
let the assumed beam-center value $C^{\text{fixed}}(\mathbf{k}_b)$ of the system array factor for the beam at $\mathbf{k}_b$ be unity.

Repeat until convergence is obtained:

LP or SOCP, fix H_2, opt H_1:

- construct a system array factor for each $\mathbf{k}_b$ using an indeterminate $H_1(\boldsymbol{f})$ and a fixed $H_2^{\text{fixed}}(\boldsymbol{f})$,
- optimize $H_1(\boldsymbol{f})$ to best meet requirements on those system array factors, using $C^{\text{fixed}}(\mathbf{k}_b)$ as convenient, and set $H_1^{\text{fixed}}(\boldsymbol{f})$ to the optimal $H_1(\boldsymbol{f})$ value,

SOCP, fix H_1, opt H_2:

choose $x_1, \ldots, x_{M_2}, \ell$ to minimize taper-loss amplitude factor ℓ such that

$H_2(0) \geq 1$ and

$$\forall \mathbf{k}_b \in \mathcal{S}, \quad \frac{\Big\| H_1^{\text{fixed}}(\cdot\,\mathbf{D})\, H_2\big((\,\cdot\, - \mathbf{k}_b)\mathbf{DR}\big)\Big\| \Big/ |C^{\text{fixed}}(\mathbf{k}_b)|}{1/\sqrt{N}} \leq \ell,$$

$$\forall \mathbf{k} \in \mathcal{I}, \left| H_1^{\text{fixed}}\big(\mathbf{kD}\big) H_2\big((\mathbf{k}-\mathbf{k}_b)\mathbf{DR}\big)\right| \leq b;$$

let $H_2^{\text{fixed}}(\boldsymbol{f}) = \big[H_2(\boldsymbol{f})\big]_{x_1,\ldots,x_{M_2}}$.

$\forall \mathbf{k}_b \in \mathcal{S}$, let $C^{\text{fixed}}(\mathbf{k}_b) = H_1^{\text{fixed}}\big(\mathbf{k}_b\mathbf{D}\big) H_1^{\text{fixed}}(0)$.

Fig. 9. The system array factor is designed by alternately optimizing $H_1(\boldsymbol{f})$ and $H_2(\boldsymbol{f})$ using linear or second-order-cone programs in each step until convergence is obtained. Optimization of $H_1(\boldsymbol{f})$ is shown in high-level pseudocode (for $H_2(\boldsymbol{f})$ it would be similar), and optimization of $H_2(\boldsymbol{f})$ is shown in detail. Figure 10 provides corresponding detail for $H_1(\boldsymbol{f})$.

LP, fix H_2, opt H_1:

choose $x_1, \ldots, x_{M_1}, g$ to minimize g such that

$$\forall \mathbf{k}_b \in \mathcal{S}, \forall \mathbf{k} \in \mathcal{G}, \quad -g \leq H_1(\mathbf{kD})\, H_2^{\text{fixed}}\big((\mathbf{k}-\mathbf{k}_b)\mathbf{DR}\big) \leq g;$$

let $H_1^{\text{fixed}}(\,\cdot\,) = \big[H_1(\,\cdot\,)\big]_{x_1,\ldots,x_{M_1}}$;

Fig. 10(a). Nth-band case. Minimizing bound g on the system array factor's grating lobes determines the subarray array factor's stopbands. The latter's passband structure then follows from the Nth-band constraint on the Nyquist sum.

SOCP, fix H_2, opt H_1:

choose $x_1, \ldots, x_{M_1}, \ell$ to minimize ℓ such that

$H_1(0) \geq 1$, and

$$\forall \mathbf{k}_b \in \mathcal{S}, \quad \frac{\Big\| H_1\big(\cdot\,\mathbf{D}\big)\, H_2^{\text{fixed}}\big((\,\cdot\, - \mathbf{k}_b)\mathbf{DR}\big)\Big\| \Big/ |C^{\text{fixed}}(\mathbf{k}_b)|}{1/\sqrt{N}} \leq \ell,$$

$$\forall \mathbf{k} \in \mathcal{G}, -g \leq H_1(\mathbf{kD})\, H_2^{\text{fixed}}\big((\mathbf{k}-\mathbf{k}_b)\mathbf{DR}\big) \leq g;$$

let $H_1^{\text{fixed}}(\,\cdot\,) = \big[H_1(\,\cdot\,)\big]_{x_1,\ldots,x_{M_1}}$;

Fig. 10(b). Non-Nth-band case. The worst of the system array factors' taper losses is minimized subject to a common fixed bound g on the peak heights of their grating lobes.

Fig. 10. Detailed optimization strategy for the Fig. 9 step, "fix H_2, opt H_1."